A Mathematical Model of the Kinetics of β-Amyloid Fibril Growth from the Denatured State

Monica M. Pallitto and Regina M. Murphy
Department of Chemical Engineering, University of Wisconsin, Madison, Wisconsin 53706 USA

ABSTRACT Spontaneous conversion of beta-amyloid peptide (Aβ) from soluble monomer to insoluble fibril may underlie the neurodegeneration associated with Alzheimer's disease. A complete description of Aβ self-association kinetics requires identification of the oligomeric species present and the pathway of association, as well as quantitation of rate constants and reaction order. Aβ was rendered monomeric and denatured by dissolution in 8 M urea, pH 10. "Refolding" and fibrillization were initiated by rapid dilution into phosphate-buffered saline, pH 7.4. The kinetics of growth were followed at three different concentrations, using size exclusion chromatography, dynamic light scattering, and static light scattering. A multi-step pathway for fibril formation and growth was postulated. This pathway included 1) rapid commitment to either stable monomer/dimer or unstable intermediate, 2) cooperative association of intermediate into a multimeric "nucleus," 3) elongation of the "nucleus" into filaments via addition of intermediate, 4) lateral aggregation of filaments into fibrils, and 5) fibril elongation via end-to-end association. Differential and algebraic equations describing this kinetic pathway were derived, and model parameters were determined by fitting the data. The utility of the model for identifying toxic Aβ oligomeric specie(s) is demonstrated. The model should prove useful for designing compounds that inhibit Aβ aggregation and/or toxicity.

NOMENCLATURE

c_{tot} = Total mass concentration of peptide;
[D] = Molar concentration (in equivalent monomers) of stable dimer;
d = Filament or fibril diameter;
d_f = Filament diameter;
d_F = Fibril diameter;
d_{sph} = Hydrodynamic diameter of a sphere with equivalent diffusivity;
D_z = Z-average translational diffusion coefficient;
$[f_i]$ = Molar concentration of filaments;
$[F_i]$ = Molar concentration of fibrils;
[I] = Molar concentration (in equivalent monomers) of amyloidogenic intermediate;
$I_b(90°)$ = Average scattered intensity of buffer at 90° scattering angle;
$I_s(90°)$ = Average scattered intensity of sample at 90° scattering angle;
I_{tol} = Average scattered intensity of toluene at 90° scattering angle;
K' = Instrument-dependent constant for light scattering analysis (Eq. 2);
k_B = Boltzmann's constant;
k_D = Rate constant, formation of stable dimer from unfolded monomer;
k_I = Rate constant, formation of amyloidogenic intermediate from unfolded monomer;
k_{ij} = Rate constant, fibril elongation by end-to-end association;
k'_{ij} = Rate constant, filament elongation by end-to-end association;
k_{la} = Rate constant, lateral aggregation of filaments to fibrils;
k_M = Rate constant, formation of stable monomer from unfolded monomer;
K_{MD} = Monomer-dimer equilibrium constant;
k_n = Forward rate constant, cooperative association of intermediate into nucleus;
k_{-n} = Reverse rate constant, disassembly of nucleus into intermediate;
k_p = Forward rate constant, addition of intermediate to nucleus or filament;
k_{-p} = Reverse rate constant, dissociation of intermediate from nucleus or filament;
L_c = Contour length (includes filaments and fibrils);
L_f = Filament length;
L_F = Fibril length;
l_k = Kuhn statistical segment length;
[M] = Molar concentration of stable monomer;
$[M_u]$ = Molar concentration of urea-unfolded monomer;
M_1 = Molecular weight of Aβ monomer;
M_{agg} = Wt-averaged molecular weight of all large aggregates;
M_f = Wt-averaged molecular weight of filaments;
M_F = Wt-averaged molecular weight of fibrils;
M_i = Molecular weight of species i;
$\langle M \rangle_w$ = Wt-averaged molecular weight (includes all species);
[N] = Molar concentration of amyloidogenic nucleus;
n = Number of intermediates in nucleus;
n_b = Refractive index of buffer;
n_{tol} = Refractive index of toluene;

Received for publication 19 March 2001 and in final form 5 June 2001.

Address reprint requests to Dr. Regina M. Murphy, Dept. of Chemical Engineering, University of Wisconsin, 1415 Engineering Dr., 3635 Engineering Hall, Madison, WI 53706. Tel.: 608-262-1587; Fax: 608-262-5434; E-mail: murphy@che.wisc.edu.

0006-3495/01/09/1805/18 $2.00

N_A = Avogadro's number;
p = Number of filaments in fibril;
$P(90°)$ = Particle scattering factor at 90° scattering angle;
$P_f(90°)$ = Particle scattering factor at 90° scattering angle for filaments;
$P_F(90°)$ = Particle scattering factor at 90° scattering angle for fibrils;
q = Reaction order, filament to fibril association;
R_{tol} = Rayleigh ratio for toluene;
T = Temperature;
w_{agg} = Weight fraction peptide in aggregated form;
w_f = Weight fraction peptide present as filaments;
w_F = Weight fraction peptide present as fibrils;
$\delta\omega_{fib}$ = Maximum allowable distance X angle between two associating fibrils;
$\delta\omega_{fil}$ = Maximum allowable distance X angle between two associating filaments;
λ_0 = Wavelength of incident light in vacuo;
λ_f = Moment of the filament distribution;
λ_F = Moment of the fibril distribution;
ρ_{lin} = Average linear density of filaments and fibrils;
v_h = Partial specific volume of hydrated peptide.

INTRODUCTION

β-Amyloid peptide (Aβ) is the major protein component of senile plaques and cerebrovascular amyloid deposits from Alzheimer's disease (AD) patients (Glenner and Wong, 1984; Masters et al., 1985). Aβ is a 39- to 43-residue proteolytic product of a membrane-associated precursor protein, APP, containing sequences from both extracellular and transmembrane regions of the parent protein (Kang et al., 1987; Masters et al., 1985). The spontaneous conversion of monomeric Aβ into fibrillar aggregates is associated with the development of Alzheimer's disease (Joachim and Selkoe, 1992). The "amyloid hypothesis," that Aβ amyloid deposition is a major causative factor in the onset of AD, is supported by biochemical, genetic, and transgenic animal studies (e.g., Yankner et al., 1990; Mattson et al., 1992; Games et al., 1995; Hsiao et al., 1996; Holcomb et al., 1998). Similar such conversions of soluble proteins or protein fragments into fibrillar polymers occur in diseases as diverse as Huntington's disease, senile systemic amyloidosis, transmissible spongiform encephalitis, and type II diabetes (Koo et al., 1999). Proteins unrelated to known disease states can be induced to form amyloid fibrils by reducing the conformational stability of the folded globular protein (Chiti et al., 2000). Indeed, it is possible to generate libraries of synthetic peptides with the tendency to self-associate into amyloid; these peptides do not share specific residue homology, but rather an alternating pattern of stretches of polar and nonpolar side chains (West et al., 1999).

Several studies suggest that Aβ is toxic only when it is aggregated (Pike et al., 1993; Simmons et al., 1994; Lorenzo and Yankner, 1994; Seilheimer et al., 1997; Hartley et al., 1999; Ward et al., 2000). This apparent link between the physical state of Aβ and its biological activity has motivated efforts to understand the kinetics and pathway of Aβ self-association. Using turbidity to measure aggregation, Jarrett et al. (1993) proposed a qualitative kinetic model for Aβ self-association. In this model, monomer is very slowly converted to an n-mer nucleus (lag phase), followed by rapid addition of monomer to the nucleus to form a fibril (linear phase), until equilibrium is reached and fibril mass concentration no longer changes (plateau phase). Tomski and Murphy (1992) used dynamic light scattering to investigate self-association kinetics of Aβ(1-40) in phosphate-buffered saline. They hypothesized that Aβ monomers spontaneously and completely converted to octamers, that the octamers stacked to form fibrils, and that longer fibrils grew by diffusion-limited irreversible end-to-end association of shorter rodlike fibrils. A quantitative mathematical model was derived to explain the data. This model accounts for changes in fibril length with time. However, it assumes complete conversion of monomer to an oligomer and therefore does not provide a mechanism whereby monomeric Aβ co-exists with fibrils at equilibrium. Furthermore, it neglects monomer addition to the fibril tip as a mechanism of growth. Naiki and Nakakuki (1996) used thioflavin T, a dye that fluoresces upon binding to amyloid fibrils, to measure fibril growth of Aβ(1-40), and proposed a simple mathematical model to explain their data. Briefly, fibril elongation was postulated to occur by reversible addition of monomer to preexisting fibrils. This model is appealing in its simplicity, but does not provide a mechanism for generation of new fibrils, nor does it simulate fibril length. Lomakin et al. (1996, 1997) used dynamic light scattering to study fibril growth from Aβ(1-40) in 0.1 M HCl and proposed a detailed kinetic model based on these data. Briefly, rapid reversible equilibration between monomers and micelles was postulated to occur, followed by spontaneous and irreversible generation of nuclei from micelles. Fibrils then grew by addition of monomer to the nucleus or fibril tip. This work represents the most detailed mathematical model of Aβ association kinetics published to date. The model accounts for the presence of both monomer and fibrillar forms, and can predict both the mass concentration of fibrils and fibril length as a function of time. However, the experiments upon which the model was based were conducted at non-physiological conditions (pH $\sim$ 1).

More recent studies have revealed that linear assemblies of Aβ are not homogeneous in structure or diameter. In electron microscopy (EM) and atomic force microscopy (AFM) studies, two types are commonly observed: 3–4-nm diameter "filaments" (also called protofilaments or protofibrils) and 8–10 nm diameter "fibrils" (Stine et al., 1996; Harper et al., 1997, 1999; Kowalewski and Holtzman, 1999; Ward et al., 2000). Some investigators have observed small globular structures that may be the building blocks for

filaments and fibrils (Stine et al., 1996; Harper et al., 1999). Malinchik et al. (1998) suggested that fibers are made of three to five laterally associated filaments, each ~3 nm in diameter. Fraser et al. (1991) observed five to six globular units with diameters of 2.5–3 nm in EM cross-sections of amyloid fibers. None of the extant kinetic models specifically includes both filament and fibril formation and growth.

In this paper we propose a detailed quantitative model for the kinetics of conversion of unfolded Aβ into fibrils. Briefly, Aβ(1-40) was denatured in 8 M urea, then rapidly diluted into phosphate-buffered saline (PBS) to initiate "refolding." Size exclusion chromatography, dynamic light scattering, and static light scattering were used to follow the monomer/oligomer/aggregate distribution and the average length, diameter, and molecular weight of aggregates as a function of time. Experiments were repeated at three different concentrations, covering a range of kinetic behavior regimes. The experimental data, together with prior published information, were used to develop a detailed kinetic model that quantitatively describes Aβ self-association kinetics from the unfolded state. Parameters were determined by nonlinear regression fitting of the model to the experimental data. The model incorporated information about both mass distribution changes and length changes, included co-existence of monomer, dimer, and aggregated species, provided mechanisms for both generation and elongation of fibrils, and explicitly accounted for filaments and fibrils. The model was able to capture all the essential features of the experimental data and represents, to our knowledge, the most detailed and complete quantitative description of Aβ kinetics at physiological conditions published to date. Besides providing a clearer mechanistic understanding of amyloid fibril growth, such models may improve our ability to design compounds that modulate fibril formation, and therefore possess therapeutic potential.

EXPERIMENTAL METHODS

Sample preparation

Urea (electrophysiology/molecular biology grade) was purchased from Boehringer-Mannheim (Indianapolis, IN). All other chemicals were purchased from Sigma-Aldrich (St. Louis, MO) unless otherwise stated. Phosphate-buffered saline with azide (PBSA; 0.01 M K_2HPO_4/KH_2PO_4, 0.14 M NaCl, 0.02% (w/v) NaN_3, pH 7.4) was double-filtered through 0.22-μm filters (Millex); 8 M urea was prepared in 10 mM glycine-NaOH buffer, pH 10, then filtered through 0.22-μm filters. Lyophilized Aβ(1-40) (Anaspec, Inc., San Jose, CA) was solubilized using pre-filtered 8 M urea, pH 10, at a concentration of 2.8 mM (70 and 140 μM final concentration) or 5.6 mM (280 μM final concentration) for 10 min. Samples were then rapidly diluted into filtered PBSA to 70, 140, or 280 μM Aβ (equivalent monomer concentration). All final solutions were at pH 7.4 and contained 0.4 M urea. (Results were not affected by increasing the incubation time in 8 M urea to 1 h, data not shown.) Samples were then filtered through 0.45 μM filters directly into light scattering cuvettes or glass vials for further analysis. MALDI-mass spectroscopy analysis confirmed that Aβ was not chemically modified by this procedure.

Size exclusion chromatography

Samples were analyzed with size exclusion chromatography (SEC) using a Superdex 75 column (Pharmacia, Piscataway, NJ) on a Pharmacia FPLC system. The mobile phase (PBSA, pH 7.4, containing 0.4 M urea) flow rate was set at 0.05 ml/min and elution peaks were detected by UV absorbance at 280 nm. The column was calibrated using the following proteins as molecular weight standards: insulin chain B (3500), ubiquitin (8500), ribonuclease A (13,700), ovalbumin (43,000), and bovine serum albumin (BSA) (67,000). To determine the distribution between small species that could be resolved on the column (MW 3-70), and larger species that could not be resolved, samples were injected without the column in place; this peak area was used to calculate the total Aβ concentration of each sample.

The column was also calibrated with 8 M urea, pH 10, (with 150 mM NaCl added to the running buffer to prevent nonspecific interactions with the column), using urea-denatured insulin chain B and ubiquitin as molecular weight markers. Mobile phase flow rate was varied from 0.05 to 0.1 ml/min. Samples of Aβ in 8 M urea, pH 10, were injected with and without the column. Apparent molecular weight was determined by comparison to the calibration data collected in the appropriate buffer, and total recovery was calculated by comparing peak areas of samples injected with and without the column in place.

Light scattering

Static and dynamic light scattering data were collected and analyzed as described previously (Shen et al., 1994). Briefly, samples in light scattering cuvettes (Hellma, NY) were placed in a temperature-controlled vat containing decahydronaphthalene. A Lexel (Fremont, CA) model 95 ion laser operated at 488 nm was focused on the cuvette and data were collected using a Malvern 4700c system (Southborough, MA). Dynamic light scattering measurements were collected at 90° scattering angle hourly or more frequently. Data were analyzed using the method of cumulants to yield a z-average translational diffusion coefficient D_z. For the purpose of reporting the data, D_z was converted to the hydrodynamic diameter of a sphere with equivalent translational diffusion coefficient, d_{sph}, using the Stokes-Einstein relationship. Average scattered intensity data at 90° scattering angle, $I_s(90°)$, were collected at the same time

intervals. For each data point intensity was measured for 10 s, and then averaged. Toluene was used as a standard reference ($R_{tol} = 39.6 \times 10^{-4}\ m^{-1}$), and the buffer intensity was also measured.

Bis-ANS fluorescence

Aβ samples were prepared as described above. Aliquots were removed at specific time intervals, then diluted into PBS, pH 7.4, such that final samples contained 2 μM Aβ, 20 μM 1,1-bis(anilino)naphthaline-5,5-disulfonic acid (bis-ANS) (Molecular Probes, Eugene, OR), and 1 mM urea. Samples were incubated at room temperature in the dark for 4 min, then analyzed for bis-ANS fluorescence intensity. Samples were excited at 360 nm, and emission spectra were taken at 450–550 nm using a PTI spectrofluorometer (South Brunswick, NJ). A background spectrum of control samples containing 20 μM bis-ANS and 1 mM urea was subtracted from each sample emission spectrum.

Cellular toxicity

Toxicity of Aβ was assessed as described in detail previously (Pallitto et al., 1999). Briefly, PC-12 cells were plated in 96-well polylysine-coated plates with ~15,000 cells/100 μL medium/well. Lyophilized Aβ was dissolved in prefiltered 8 M urea, pH 10, at 12 mg/ml for 10 min, then diluted to 70, 140, or 280 μM with sterile-filtered PBS. The samples were allowed to aggregate for 1 or 3 days at 25°C, then diluted to 35 μM with fresh media and added to plated cells. Plates were incubated for 24 h at 37°C, then toxicity was assessed using the 3-(4-,5 dimethylthiazol-2-yl)-2,5 diphenyltetrazolium bromide (MTT) assay. All final solutions (including controls) contained 0.4 M urea.

EXPERIMENTAL RESULTS

Unfolding of Aβ in urea

To create a mathematical model of the kinetics of Aβ aggregation, we needed a well-characterized and reproducible initial condition. The initial state of synthetic Aβ is poorly defined; the method of synthesis, the lyophilization conditions, and the solvent used to dissolve the peptide all influence the starting conformation and aggregation state (Barrow et al., 1992; Shen and Murphy, 1995; Thunecke et al., 1998). For our studies, the preferred state was completely monomeric and unfolded. We chose 8 M urea, pH 10, as a starting solvent because 8 M urea usually unfolds polypeptides to the random coil state (Creighton, 1994), and because Aβ aggregation is hindered at pH $>$ 9 (Burdick et al., 1992). Furthermore, refolding of proteins from the urea-denatured state is a widely used technique in protein-refolding kinetic studies (Goldberg et al., 1991; Fink, 1998).

Aβ(1-40) in 8 M urea, pH 10, eluted as a single sharp symmetric peak on a calibrated size exclusion column with a residence time equivalent to 5.3-6.6 kDa (compared to its known molecular weight of 4.3). The apparent molecular weight was sensitive to the mobile phase flow rate, decreasing with increasing flow rate. This sensitivity to flow rate is likely due to the presence of NaCl in the mobile phase, but not in the sample; NaCl facilitates aggregation of Aβ (data not shown) but reduces nonspecific interactions with the column. Recovery of injected Aβ in the monomer peak was complete within experimental error: at a concentration of 120 μM, 99 $\pm$ 4% (SEM) was recovered, and at 2.8 mM, 97 $\pm$ 4% was recovered. The intensity of scattered light from Aβ(1-40) in 8 M urea, pH 10, was not greater than solvent alone, and there was no change in scattered intensity over a 24-h period, further indicating the absence of aggregate. Circular dichroic spectra contained no strong bands, and in particular lacked any trace of a minima at 218 nm or 222 nm, consistent with a lack of β-sheet or α-helix; however, the strong absorbance of urea precluded collection of reliable spectral data below 210 nm, and therefore more definitive secondary structure assignments could not be made. Together, these data indicate that 8 M urea, pH 10, is an effective solvent, and renders Aβ completely monomeric and unfolded.

Aβ monomer/oligomer size distribution in PBSA

Refolding was initiated by rapid dilution of urea-denatured Aβ(1-40) into PBSA. The resulting solution was analyzed with size exclusion liquid chromatography (SEC). Representative chromatograms are shown in Fig. 1. Invariably, two peaks were observed in the inclusion volume of the column, eluting with retention times corresponding to molecular masses of 4.1 $\pm$ 0.2 and 9.5 $\pm$ 0.2 kDa. These peaks will be referred to as monomer and dimer, respectively. A peak that eluted at the void volume was observed, but not consistently. No difference in chromatograms was observed when the sample was centrifuged before injection (data not shown).

The identical samples were injected using the same sample loop and detector, but without the column in place, to measure the total concentration (total peak area) of Aβ. To calculate the fraction of Aβ in monomer and dimer populations, the individual peak areas (obtained with the column in place) were divided by the peak area without the column. The fraction of aggregates ($>$70 kDa) was calculated by difference. A summary of the concentrations of monomer, dimer, and aggregates is given in Table 1. These values did not change appreciably over time, up until precipitates were visible (data not shown). A weighted nonlinear regression fit to the data yields a relationship between monomer and dimer of $[D] = 0.6 \pm 0.3[M]^{2\pm0.2}$. The second-order dependence on concentration is consistent with assignment of the two peaks as monomer and dimer.

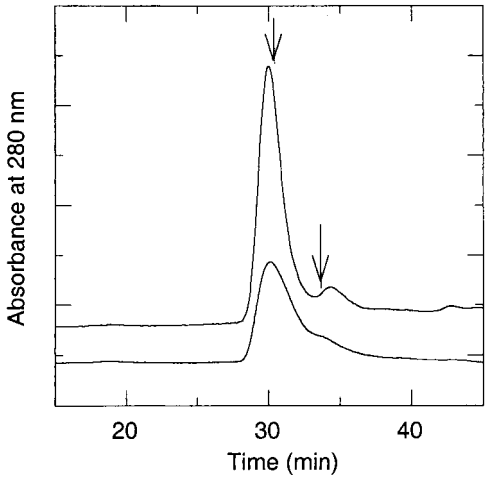

FIGURE 1 Representative chromatograms of Aβ in PBSA. Lyophilized Aβ was dissolved in 8 M urea, pH 10, diluted at least 20-fold into PBSA, then injected onto a Superdex 75 column. Running buffer was PBSA with 0.4 M urea; flow rate was 0.05 ml/min. Peak detection was by absorbance at 280 nm. Arrows indicate predicted retention times for monomer and dimer, based on column calibration.

Aβ aggregate growth kinetics

Dilution of urea-denatured Aβ into PBSA produced aggregates possessing a linear stiff or semiflexible morphology (Murphy and Pallitto, 2000). We examined changes in size of Aβ aggregates as a function of time and concentration. Aggregate size was characterized by measuring D_z and converting this to the average hydrodynamic diameter d_{sph}, which is sensitive to the average length of the aggregates. (Scattering from monomer/dimer populations is too weak to be detected in the presence of aggregates.) These data were previously reported (Murphy and Pallitto, 2000) and are shown in Fig. 2. Within a few minutes of dilution of urea-denatured Aβ into PBSA, large aggregates were already present. Interestingly, aggregates were initially largest at the lowest concentration (70 μM Aβ). Patterns of growth were strongly concentration-dependent. At 70 μM, d_{sph} was nearly constant. At 140 and 280 μM, initial sizes were about the same ($d_{sph} \sim 25$ nm); both increased, but the rate of increase was much faster at 280 μM.

TABLE 1 Size distribution as function of total Aβ concentration

Nominal Concentration* (μM)	Measured Concentration (μM)	Monomer (μM)	Dimer (μM)	Aggregate (μM)
70	60 ± 2	7 ± 1	33 ± 3	20 ± 4
140	123 ± 7	11 ± 2	67 ± 8	46 ± 9
280	260 ± 20	13.6 ± 0.3	130 ± 10	120 ± 10

*All concentrations are given in equivalent monomer concentration. The nominal concentration was calculated based on weighing out a specified amount of lyophilized peptide. The measured concentration was determined from the peak area of the sample injected onto the FPLC system without the column in place, using an extinction coefficient of 0.3062 $(mg/ml)^{-1}$ cm^{-1} (Simmons et al., 1994).

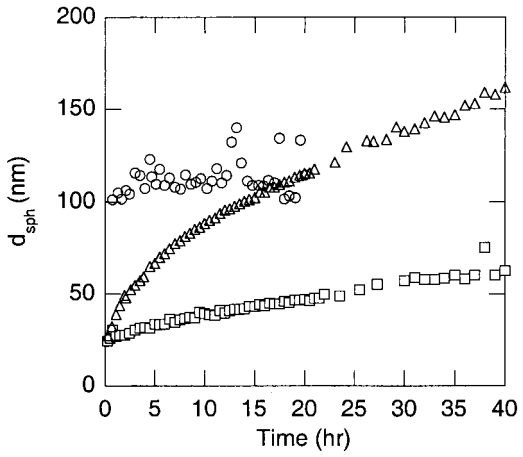

FIGURE 2 Average hydrodynamic diameter (d_{sph}) as a function of time and concentration for 70 μM (○), 140 μM (□), and 280 μM (△) Aβ (nominal concentration, equivalent monomers). Aβ was prepared as described above; autocorrelation functions were collected at 90° scattering angle and analyzed as described in the text.

Average scattering intensity at 90° scattering angle, $I_s(90°)$, was measured at the same time intervals. $I_s(90°)$ is sensitive to the average molecular weight of the aggregates. Both the absolute intensity and the rate of change were dramatically dependent on Aβ concentration (Fig. 3). At 70 μM, $I_s(90°)$ was relatively constant with time. At 140 μM, $I_s(90°)$ slowly doubled over the course of 24 hours. At 280 μM, $I_s(90°)$ increased ~6-fold over ~10 h, then leveled off. $I_s(90°)$ is related to the size and shape of the particles in solution as (Shen et al., 1994):

$$I_s(90°) = K' c_{tot} \langle M \rangle_w P(90°) + I_b(90°) \quad (1)$$

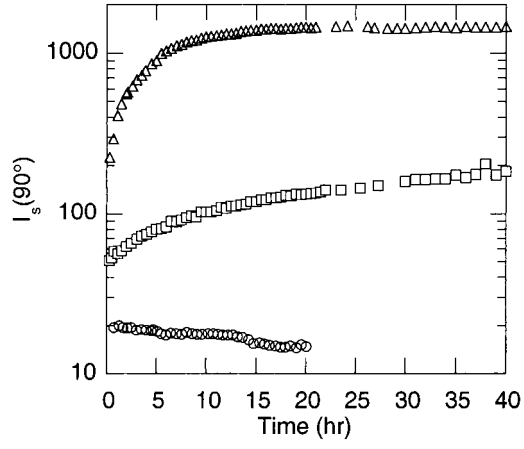

FIGURE 3 Average scattering intensity $I_s(90°)$ for 70 μM (○), 140 μM (□), and 280 μM (△) Aβ. Samples are identical to those described in Fig. 2.

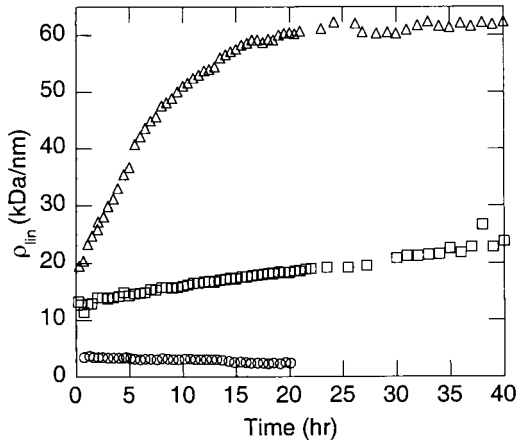

FIGURE 4 Linear density ρ_{lin} as a function of time and concentration for 70 μM (○), 140 μM (□), and 280 μM (△). ρ_{lin} was calculated from d_{sph} and $I_s(90°)$ as described in the text.

where c_{tot} = total peptide concentration, $\langle M\rangle_w$ is the weight-averaged molecular weight of particles in solution, $P(90°)$ is the particle scattering factor at 90°, $I_b(90°)$ is the scattered intensity of the buffer, and K' is an instrument-dependent constant,

$$K' = \frac{4\pi^2 n_b^2 \left(\frac{dn}{dc}\right)^2}{N_A \lambda_o^4} \frac{I_{tol}}{R_{tol}} \frac{n_{tol}}{n_b} \qquad (2)$$

where n_b and n_{tol} are the refractive indices of buffer and toluene, respectively, dn/dc is the refractive index increment (0.145 ml/g), N_A is Avogadro's number, λ_0 is the laser wavelength in vacuo, I_{tol} is the scattered intensity from a toluene sample, and R_{tol} is the Rayleigh ratio for toluene.

Results from SEC and light scattering measurements were combined to evaluate the average linear density ρ_{lin} (mass per unit length, M_{agg}/L_c) of the linear aggregates as follows. If only monomer, dimer, and large aggregates are present, then $\langle M\rangle_w = \Sigma w_i M_i \sim w_{agg} M_{agg}$, with $\langle M\rangle_w$ related to $I_s(90°)$ per Eq. 1 and w_{agg} given in Table 1. The fibril contour length L_c was calculated from the measured d_{sph} along with an experimental estimate of fibril flexibility (Kuhn statistical length l_k = 180 nm, Murphy and Pallitto, 2000), using relations derived by Yamakawa and Fujii (1973). $P(90°)$ was calculated from L_c and l_k, using the theory derived by Koyama (1973) and described in Shen et al. (1994). Then,

$$\rho_{lin} = \frac{M_{agg}}{L_c} = \left(\frac{I_s(90°) - I_b(90°)}{K' c_{tot} P(90°)}\right)\left(\frac{1}{w_{agg}}\right)\left(\frac{1}{L_c}\right) \qquad (3)$$

ρ_{lin}, a measure of the thickness of the chains, is shown in Fig. 4. At 70 μM, ρ_{lin} was nearly constant over time with an initial value of ~4 kDa/nm. At 140 μM, ρ_{lin} was higher than at 70 μM (13 kDa/nm) initially, and increased modestly over time. The most dramatic changes were observed at the highest concentration, 280 μM; ρ_{lin} was greater than the other concentrations initially (20 kDa/nm), and increased rapidly over the first ~8 h, then leveled out after ~20 hours at ~60 kDa/nm.

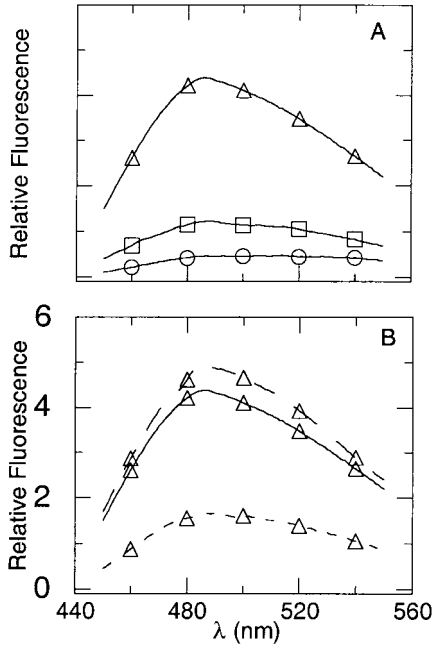

FIGURE 5 Bis-ANS fluorescence spectra in the presence of 2 μM Aβ. Aβ samples were prepared at 70, 140, or 280 μM as described above, then diluted at the indicated time into a solution containing 20 μM bis-ANS. Excitation wavelength was 360 nm and a background spectrum was subtracted. Binding of bis-ANS to hydrophobic sites produces an increase in fluorescence intensity and a blue-shifting of the emission maximum to ~480–490 nm. (*A*) Sample aggregated at 70 μM (○), 140 μM (□), and 280 μM (△), then diluted to 2 μM, taken 4 h after sample preparation. (*B*) Sample aggregated at 280 μM (△), then diluted to 2 μM, taken 1 h (*short dashed line*), 4 h (*solid line*), or 2 days (*long dashed line*) after sample preparation.

Aggregate hydrophobicity

The fluorescent dye bis-ANS was used as a qualitative probe for exposed hydrophobic surfaces on Aβ aggregates. The dye binds to exposed hydrophobic patches on partially folded proteins, leading to an increase in fluorescence intensity and blue-shifting of the emission maximum (Gibbons and Horowitz, 1995). Freshly-diluted monomeric Aβ does not cause bis-ANS fluorescence (Kremer et al., 2000). Aβ was aggregated at 70, 140, or 280 μM, then diluted to 2 μM into a solution containing bis-ANS. In Fig. 5 *A* Bis-ANS fluorescence is shown as a function of the concentration at which Aβ was aggregated. At 70 μM a fluorescence peak was observed, which did not change appreciably with time (data not shown). At 140 μM, the peak fluorescence is ~2–3-fold higher, and at 280 μM, the fluorescence increased another 3–4-fold and is slightly

blue-shifted. At 280 μM (Fig. 5 *B*) and, to a lesser extent, at 140 μM (not shown), fluorescence intensity increased over the first few hours, then stabilized. These data suggest that there are distinct structural differences between the aggregates formed at these different concentrations.

MATHEMATICAL MODEL

Experimental results described above lay the foundation for developing a mathematical model of Aβ self-association kinetics. The key observations that the model must capture are:

1. A substantial amount of material remained in a nonfibrillar state, as monomers and dimers, after renaturation. Dimer-monomer concentrations were related by a second-order function;
2. High-molecular-weight species formed very rapidly upon dilution;
3. The initial aggregate size was greatest at the lowest test concentration;
4. The rate of growth increased with concentration;
5. The linear density of aggregates increased at higher concentrations with time, eventually reaching a steady-state value;
6. Aggregates formed at different concentrations are structurally distinct, specifically in terms of exposed hydrophobic regions.

The development of the structure of the model will be discussed first, followed by a description of the detailed equations derived to solve the model.

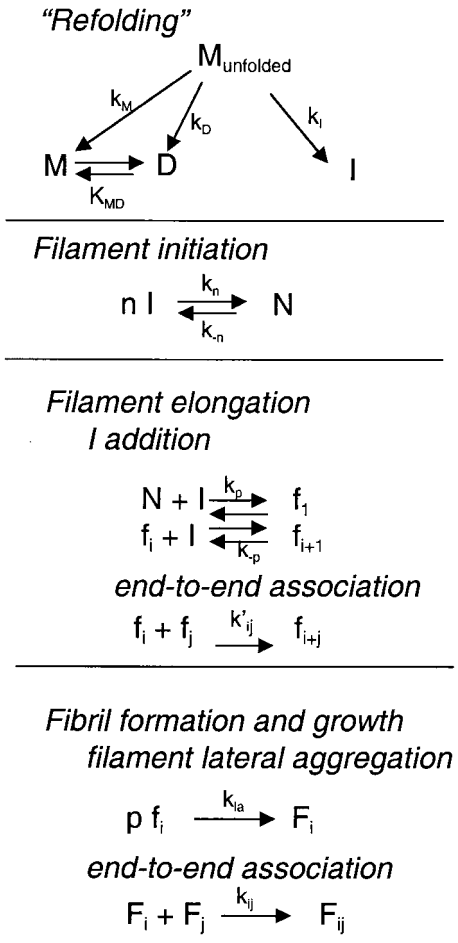

FIGURE 6 Schematic of model describing kinetics of Aβ fibril growth.

Monomer, dimer, and aggregate mass distribution

We observed that 1) monomer and dimer concentrations depended on total Aβ concentration; 2) monomer, dimer, and aggregate distribution was relatively constant with time; and 3) large aggregates appeared very quickly upon dilution into PBSA. We used these data to postulate that "refolding" of Aβ from the urea-denatured state occurs extremely rapidly, and that refolded species become quickly and irreversibly committed to either monomer/dimer (nonamyloid) or aggregate (amyloid) status. A division between amyloidogenic and nonamyloidogenic populations of Aβ has previously been postulated by Soto and Castano (1996), and is conceptually similar to the division between aggregated and correctly folded proteins observed in other protein refolding studies (Goldberg et al., 1991). We also observed that monomer and dimer concentrations were related by a simple second-order equation, and therefore propose that monomer and dimer are in rapid reversible equilibrium. Schematically this is shown in Fig. 6 under the "refolding" step, where M_{unfold} represents monomeric Aβ in its urea-denatured state, *M* and *D* are monomer and dimer "native" conformations that are stable in PBSA, respectively, and *I* is an unstable intermediate that can form larger aggregates. In the refolding literature *M* and *D* formation would be considered "on-pathway" and $I \rightarrow$ aggregate would be "off-pathway." The split between amyloidogenic and nonamyloidogenic populations was assumed to be irreversible.

We considered, and discarded, several alternative schemes in which monomers (and/or dimers) were assumed to be all "off-pathway", e.g., $M \rightarrow D \rightarrow I \rightarrow$ aggregates. For example, conversion to aggregates could occur via cooperative association of monomer (or dimer) to reactive intermediate. This model is similar to that proposed by Jarrett et al. (1993) and Lomakin et al. (1996, 1997). Under this model, [I] remains very small until the "critical concentration" of [M] is reached, then [M] remains constant (and equal to this critical concentration) as total Aβ concentration is increased. We instead observed an increase in [M] and [D] as the total concentration increased, directly contradicting this model. Two other models, used commonly to describe linear polymerization processes (Billmeyer, 1971; Schmidt, 1998), were explored. Aβ association was postulated to occur either via a stepwise (condensation) polymer-

ization scheme, in which any two oligomeric species react to form longer polymers, or via addition (chain) polymerization, in which a highly reactive initiator is formed and monomers quickly add to the growing chain. With stepwise polymerization, the molecular weight distribution is very broad, and very few monomers are present for even modest degrees of aggregation. This model is inconsistent with experimental data. Chain polymerization produces a distribution that includes only monomer and high-molecular-weight polymer, which is closer to the observed distribution. However, the monomer concentration tends toward a constant value, independent of total concentration, in contrast to observation. Several variants of these ideas were evaluated; none were fully consistent with experimental data. Therefore, we conclude that formation of nonamyloid and amyloid Aβ species occurs in parallel, not serial, fashion.

Aggregate size and shape

Two key structural features that have been consistently observed in AFM studies are "filaments" of 3–4-nm thickness and "fibrils" of 8–12-nm thickness (Stine et al., 1996; Harper et al., 1997, 1999). Cross-section EM images and x-ray diffraction studies indicate that fibrils contain three to six laterally associated filaments (Fraser et al., 1991; Malinchik et al., 1998). Analysis of the light scattering data revealed increases in ρ_{lin} with concentration and with time, and substantially greater (~3-fold) steady-state ρ_{lin} at 280 μM relative to initial values. Given these data and the aforementioned EM, AFM, and XRD studies, we incorporated into our model two possible long linear aggregated structures: filaments (thin) and fibrils (thick).

Development of the detailed kinetic model for filament and fibril formation and elongation relied on several key experimental observations. First, we observed that even at the earliest time points high-molecular-weight aggregates were present, and that the initial size (d_{sph}) was greatest at the lowest concentration. We postulated that this could occur due to a nucleation-dependent process akin to crystallization, where fewer longer crystals are observed at lower concentrations and more, shorter crystals are observed at higher concentrations (Jarrett et al., 1993). Thus, a nucleation mechanism was applied not to the initial partitioning between *M*/*D* and *I*, but to further self-association of *I* into larger species. A high-order, cooperative reaction is necessary to capture the inverse relationship between initial size and concentration. We modeled filament initiation as reversible self-association of *I* to form a nucleus, *N*, containing *n I*, characterized by forward and reverse rate constants k_N and k_{-N}, respectively. This step is illustrated in Fig. 6 as filament initiation. We further assumed that nuclei *N* could elongate into filaments *f* by addition of *I*. This is illustrated in Figure 6 as filament elongation by *I* addition.

The second key observation was the significant increase in ρ_{lin} at 280 μM with time, whereas at 70 μM ρ_{lin} was constant and small. We postulated that the increase in ρ_{lin} at 280 μM was due to lateral aggregation of several filaments into fibrils. This would be consistent with observations indicating that fibrils are close-packed filaments (Fraser et al., 1991; Malinchik et al., 1998) and would have a high reaction order, to explain the strong concentration dependence. Therefore filaments *f* were assumed to laterally associate into fibrils *F*, as shown in Fig. 6. Lateral association was assumed to be irreversible, characterized by a rate constant k_{la}.

Third, we observed an increase in d_{sph} without a corresponding increase in ρ_{lin} at 280 μM and longer times ($t >$ ~20 h, see Figs. 2 and 4). The increase in d_{sph} indicates an increase in fibril length. No change in ρ_{lin} implies a constant fibril diameter. We postulated that the increase in d_{sph} at $t >$ ~20 h was due to axial elongation by end-to-end association of shorter fibrils. Additional experimental evidence of this was presented in Murphy and Pallitto (2000) and Harper et al. (1999). End-to-end association was assumed to be slow and diffusion-limited and was modeled after the classic Smoluchowski equation. The rate constant associated with end-to-end association, k_{ij}, was assumed to depend on length as (Hill, 1983, Tomski and Murphy, 1992):

$$k_{ij} = \frac{k_B T}{3\eta}\frac{N_A}{1000}\frac{\delta^2\omega^2}{L_i + L_j}\left(\frac{\ln(L_i/d) + v_i}{L_i} + \frac{\ln(L_j/d) + v_j}{L_j}\right)$$

$$v_i = 0.312 + 0.565(L_i/d)^{-1} - 0.100(L_i/d)^{-2}, \quad (4)$$

where *i* and *j* indicate the size of associating fibrils, k_B is the Boltzmann constant, *T* is the absolute temperature, η is the solvent viscosity, δ is the maximum allowable distance between two fibril ends, ω is the maximum allowable angle between two fibrils, L_i is the fibril (or filament) length, and *d* is the fibril (or filament) diameter. For completeness, a similar mechanism for end-to-end association of filaments was included. End-to-end association was assumed to be an irreversible process.

Model equations

The schematic depicted in Fig. 6 and justified in detail in the previous sections was used to derive a set of equations describing the kinetics of Aβ aggregation. Refolding of denatured peptide to produce *M*, *D*, and *I* was described by simple irreversible kinetic expressions:

$$\frac{d[M]}{dt} = k_M[M_u] \quad (5)$$

$$\frac{d[D]}{dt} = k_D[M_u]^2 \quad (6)$$

$$\frac{d[I]}{dt} = k_I[M_u]^2, \quad (7)$$

where $[M_u]$ is the concentration of monomer in the urea-unfolded state. The initial distribution among M, D, and I was assumed to occur very rapidly, relative to further I association. The data were best modeled if I was assumed to be dimeric, hence the form of Eq. 7. Equations 5–7 were solved to give a pseudo-steady-state expression for [I], i.e., the value that would be obtained at long times if there were no further aggregation of I:

$$[\mathrm{I}] = 2\left(\frac{k_\mathrm{I}}{k_\mathrm{I}+k_\mathrm{D}}\right)\left(\frac{[\mathrm{M_u}]_0}{2} - \frac{k_\mathrm{M}}{4(k_\mathrm{I}+k_\mathrm{D})} \times \ln\left[1 + \frac{2(k_\mathrm{I}+k_\mathrm{D})[\mathrm{M_u}]_0}{k_\mathrm{M}}\right]\right), \quad (8)$$

where $[M_u]_0$ is the initial Aβ concentration in the unfolded state. The amount of M and D formed is simply:

$$[\mathrm{M}] + [\mathrm{D}] = [\mathrm{M_u}]_0 - [\mathrm{I}] \quad (9)$$

We assumed that "native" monomer M and dimer D were always in equilibrium:

$$K_\mathrm{md} = \frac{[\mathrm{D}]}{[\mathrm{M}]^2} \quad (10)$$

Equations 8–10 give the initial concentrations of M, D, and I just after dilution into PBSA. For convenience, M, D, and I concentrations are given in equivalent monomer molar concentrations.

I is consumed by initiation and elongation steps (Fig. 6) and associates to form N, or adds to N to form filaments, or adds to filaments to increase their length. The shortest filament is produced by addition of I to N and is referred to as f_{n+1}. Filaments can be any size i from $(n+1)$ to ∞, where n is the number of I per N. (There are $2i$ monomers per filament f_i.) Summing over all species gives:

$$\frac{d[\mathrm{N}]}{dt} = k_\mathrm{n}[\mathrm{I}]^\mathrm{n} - k_{-\mathrm{n}}[\mathrm{N}] - k_\mathrm{p}[\mathrm{I}][\mathrm{N}] + k_{-\mathrm{p}}[f_{\mathrm{n}+1}] \quad (11)$$

$$\frac{d[\mathrm{I}]}{dt} = -nk_\mathrm{n}[I]^\mathrm{n} + nk_{-\mathrm{n}}[\mathrm{N}] - k_\mathrm{p}[\mathrm{I}]\left\{[\mathrm{N}] + \sum_{\mathrm{i}=\mathrm{n}+1}^{\infty}[f_\mathrm{i}]\right\} + k_{-\mathrm{p}}\sum_{\mathrm{i}=\mathrm{n}+1}^{\infty}[f_\mathrm{i}] \quad (12)$$

A filament of length i, f_i, is formed by addition of I to f_{i-1} or by end-to-end association of two shorter filaments (f_j and f_k, where $j + k = i$); f_i is lost by similar reactions: addition of I to form f_{i+1}, or end-to-end association with any filament f_j to form filaments of length $i + j$. In addition, filaments are lost by (irreversible) lateral aggregation to fibrils. Mathematically, this is expressed as:

$$\frac{d[f_\mathrm{i}]}{dt} = k_\mathrm{p}[\mathrm{I}]\{[f_{\mathrm{i}-1}] - [f_\mathrm{i}]\} - k_{-\mathrm{p}}\{[f_\mathrm{i}] - [f_{\mathrm{i}+1}]\} - pk_\mathrm{la}[f_\mathrm{i}]\left(\sum_{\mathrm{j}=\mathrm{n}+1}^{\infty}[f_\mathrm{j}]\right)^{\mathrm{q}-1} - \sum_{\mathrm{j}=\mathrm{n}+1}^{\infty}k'_{\mathrm{ij}}[f_\mathrm{i}][f_\mathrm{j}] + \frac{1}{2}\sum_{\mathrm{j}=\mathrm{n}+1}^{\mathrm{i}-(\mathrm{n}+1)}k'_{\mathrm{j,i-j}}[f_\mathrm{j}][f_{\mathrm{i}-\mathrm{j}}] \quad (13)$$

where p is the number of filaments per fibril, q is the order of the lateral association reaction, k_{la} is the lateral association rate constant (assumed independent of length), and k'_{ij} and k'_{jk} are end-to-end association rate constants for filaments (defined in Eq. 5). Since i varies from $n + 1$ to ∞, there are an infinite number of equations like Eq. 13. To make this system of equations finite, we defined moments of the filament size distribution $\lambda_{f\alpha}$:

$$\lambda_{\mathrm{f}\alpha} = \sum_{\mathrm{i}=\mathrm{n}+1}^{\infty} i^\alpha[f_\mathrm{i}] \quad (14)$$

Fibrils form by lateral association of filaments and grow in length by end-to-end association of shorter fibrils. We defined moments of the fibril size distribution $\lambda_{F\alpha}$:

$$\lambda_{\mathrm{F}\alpha} = \sum_{\mathrm{i}=\mathrm{n}+1}^{\infty} i^\alpha[F_\mathrm{i}], \quad (15)$$

and assumed that the length of fibrils formed by lateral association was equal to the number-average length of filaments at that time. Substituting in the definition of moments (Eqs. 14 and 15) into Eqs. 12 and 13, and similarly deriving equations for fibril formation and growth, produces a finite set of coupled differential equations:

$$\frac{d[\mathrm{I}]}{dt} = -nk_\mathrm{n}[\mathrm{I}]^\mathrm{n} - nk_{-\mathrm{n}}[N] - k_\mathrm{p}[\mathrm{I}]\{[\mathrm{N}] + \lambda_{\mathrm{f}0}\} + k_{-\mathrm{p}}\lambda_{\mathrm{f}0} \quad (16)$$

$$\frac{d\lambda_{\mathrm{f}0}}{dt} = k_\mathrm{p}[\mathrm{N}][\mathrm{I}] - k_{-\mathrm{p}}[f_{\mathrm{n}+1}] - pk_\mathrm{la}\lambda_{\mathrm{f}0}^\mathrm{q} - \frac{1}{2}\overline{k'_{\mathrm{ij}}}\lambda_{\mathrm{f}0}^2 \quad (17)$$

$$\frac{d\lambda_{\mathrm{f}1}}{dt} = k_\mathrm{p}[\mathrm{I}]\{(n+1)[\mathrm{N}] + \lambda_{\mathrm{f}0}\} - k_{-\mathrm{p}}\{n[f_{\mathrm{n}+1}] + \lambda_{\mathrm{f}0}\} - pk_\mathrm{la}\lambda_{\mathrm{f}1}\lambda_{\mathrm{f}0}^{\mathrm{q}-1} \quad (18)$$

$$\frac{d\lambda_{\mathrm{f}2}}{dt} = k_\mathrm{p}[\mathrm{I}]\{(n+1)^2[\mathrm{N}] + 2\lambda_{\mathrm{f}1} + \lambda_{\mathrm{f}0}\} - k_{-\mathrm{p}}\{n^2[f_{\mathrm{n}+1}] + (\lambda_{\mathrm{f}0} - \lambda_{\mathrm{f}1})\} - pk_\mathrm{la}\lambda_{\mathrm{f}2}\lambda_{\mathrm{f}0}^{\mathrm{q}-1} + \overline{k'_{\mathrm{ij}}}\lambda_{\mathrm{f}1}^2 \quad (19)$$

$$\frac{d\lambda_{\mathrm{F}0}}{dt} = k_\mathrm{la}\lambda_{\mathrm{f}0}^\mathrm{q} - \frac{1}{2}\overline{k_{\mathrm{ij}}}\lambda_{\mathrm{F}0}^2 \quad (20)$$

$$\frac{d\lambda_{F1}}{dt} = pk_{la}\lambda_{f1}\lambda_{f0}^{q-1} \tag{21}$$

$$\frac{d\lambda_{F2}}{dt} = p^2k_{la}\lambda_{f2}\lambda_{f0}^{q-1} + \overline{k_{ij}}\lambda_{F1}^2, \tag{22}$$

where $\overline{k'_{ij}}$ are $\overline{k_{ij}}$ were calculated from Eq. 4 using the number average length of filaments or fibrils, respectively.

Parameter estimation procedure

Equations 16–22 together with Eq. 11 were solved numerically using the program DDASAC (Caracotsios and Stewart, 1985). Model parameters were derived by fitting experimental data to model equations, using the parameter estimation package GREG (Stewart, 1987) and the following procedure.

First, we determined the "refolding" parameters. Estimates of $K_{md} = 0.64 \pm 0.08\ \mu M^{-1}$, $k_M/k_I = 80 \pm 30\ \mu M$, and $k_D/k_I = 0.65 \pm 0.15$ were obtained by nonlinear regression fit of the data in Table 1 to Eqs. 8–10. Because these are rapid reactions, only the ratios of rate constants, rather than the absolute values, could be evaluated. As shown in Fig. 7, the model calculations accurately reflect the observed population distribution at all three concentrations tested. We considered and discarded mechanisms in which k_M or k_D was set equal to zero, because these were not able to capture the observed trends satisfactorily (not shown). Addition of the extra parameter is statistically justified at the 99.5% level, using the F-statistic (Davies, 1954).

Second, we determined the parameters involved in filament initiation and elongation. To compare experimental data to model simulations, a method was developed that relates the experimental observations d_{sph} and $I_s(90)$ to the size distributions calculated from the model. The weight-average-molecular-weight of filaments M_f and fibrils M_F were related to model-generated distributions as:

$$M_f = 2M_1\frac{\lambda_{f2}}{\lambda_{f1}}$$

$$M_F = 2M_1\frac{\lambda_{F2}}{\lambda_{F1}} \tag{23}$$

where M_1 is the monomer molecular weight. Filament and fibril lengths were calculated assuming a solid cylindrical geometry:

$$L_f = \frac{4v_hM_f}{\pi d_f^2N_A}$$

$$L_F = \frac{4v_h}{\pi d_f^2N_A}\frac{M_F}{p}, \tag{24}$$

where the hydrated specific volume v_h was set equal to 1.1 cm^3/g (Tomski and Murphy, 1992), and the filament diameter d_f was set equal to 4 nm (Harper et al., 1999). $d_{sph,f}$ and $d_{sph,F}$ were calculated from L_f and L_F, respectively, as described in Shen et al. (1994). The inverse z-averaged d_{sph} was then calculated from:

$$d_{sph} = \left(\frac{w_fM_f(d_{sph,f})^{-1} + w_FM_F(d_{sph,F})^{-1}}{w_fM_f + w_FM_F}\right)^{-1} \tag{25}$$

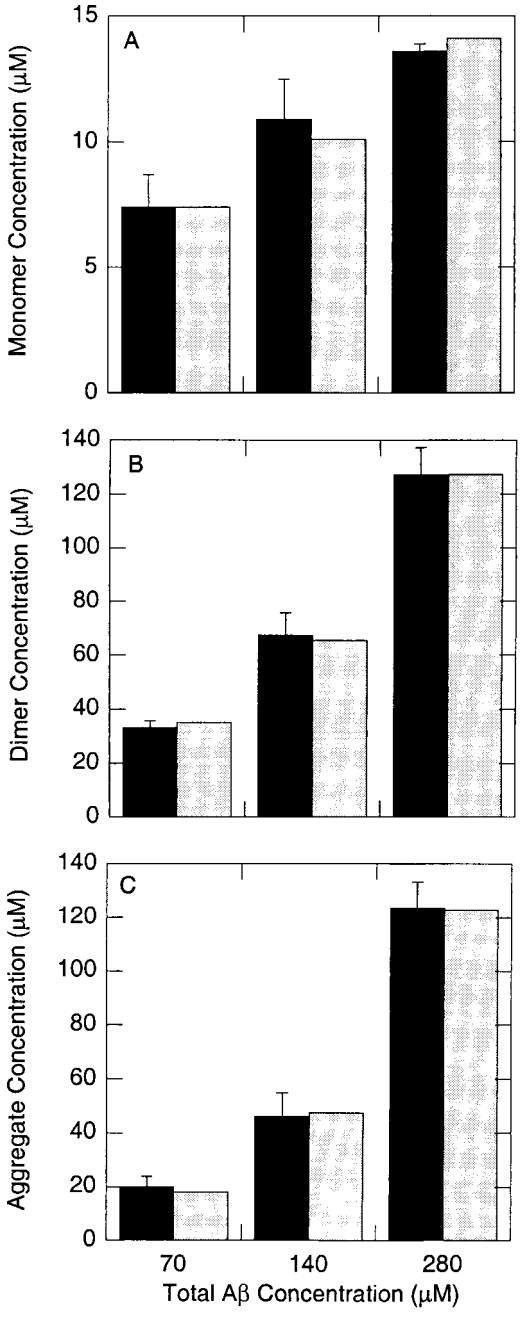

FIGURE 7 Observed (*dark shading*) and simulated (*lightly shaded*) weight fraction of (*A*) monomer, (*B*) dimer, and (*C*) aggregate. Samples were prepared at the indicated total Aβ concentration; distributions were evaluated from size exclusion chromatograms. Concentrations are given as equivalent monomer concentrations.

where w_f and w_F are the weight fractions of filament and fibril, respectively, calculated from the model. In sum, Eqs. 23–25 allow a direct comparison between experimentally obtainable values and model calculations of d_{sph}.

$I_s(90°)$ was related to the distribution as follows. The weight-average molecular weight $\langle M \rangle_w$ of the entire sample was determined from:

$$\langle M \rangle_w = \frac{[M] + 4([D] + n^2[N] + \lambda_{f2} + \lambda_{F2})}{[M] + 2([D] + n[N] + \lambda_{f1} + \lambda_{F1})} M_1 \quad (26)$$

L_f and L_F were used to calculate the particle scattering factors, $P_f(90°)$ and $P_F(90°)$, for filaments and fibrils, respectively (Koyama, 1973; Shen et al., 1994), assuming $l_k = 180$ nm for both filaments and fibrils (Murphy and Pallitto, 2000). The overall scattering factor $P(90°)$ was determined by averaging the individual values (Burchard, 1983):

$$P(90°) = \frac{w_f M_f P_f(90°) + w_F M_F P_F(90°)}{w_f M_f + w_F M_F}. \quad (27)$$

The scattered intensity was calculated from Eqs. 9, 26, and 27. Together, Eqs. 24, 26, and 27 relate experimentally observable values of $I_s(90°)$ to size distributions calculated from the model.

As previously discussed, at 70 μM the values of d_{sph} and $I_s(90°)$ indicated large aggregates were present very soon after dilution into folding buffer. Furthermore, d_{sph} and $I_s(90°)$ at 70 μM did not change with time. We interpreted this to indicate 1) that filament initiation and filament elongation by *I* addition was rapid, and 2) that slower growth by end-to-end association or lateral association was negligible at this concentration. Given this, initial estimates of parameter values were obtained from the experimental data at 70 μM by setting all parameters except k_n, k_p, and n equal to zero and by neglecting time-dependent terms in Eqs. 11 and 16–22. These simplified equations together with Eqs. 23–25 give d_{sph} as a function of the ratio k_n/k_p and n. We fixed n, and found the best-fit value for k_n/k_p by comparing observed and calculated values for initial d_{sph}. This procedure was repeated for varying choices of n. Then, these sets of (n, k_n/k_p) were used along with the model equations to calculate the initial d_{sph} at the two higher concentrations. Closest agreement with all three concentrations was obtained with $n = 6$ and $k_n/k_p = 1.7 \times 10^{-6}$ μM^{-4}. This result indicates that 6 *I* cooperatively associate to form *N*, with a sixth-order dependence on concentration of *I*.

Lastly, we determined the parameters describing lateral association and end-to-end axial elongation. For this, k_{-n} and k_{-p} were kept close to zero. This is equivalent to assuming that filament initiation and elongation are essentially irreversible; subsequent calculations indicated that small changes in the chosen rate constants did not change the model output (not shown) and that no unique values for these reverse rate constants could be ascertained from the data. Three kinetic rate constants, k_{ij}, k'_{ij}, k_{la}, plus p and q remained to be determined. We fixed p and q arbitrarily to different integer values between 2 and 6, based on reports that fibrils contained three to six subunits (Fraser et al., 1991; Malinchik et al., 1998), then fitted kinetic rate constants at given values of p and q by weighted multi-parameter nonlinear regression to the d_{sph} and $I_s(90°)$ data at both 140 and 280 μM. The "best" parameter set was chosen as that which gave the lowest sum of squares of the residuals. The data were best fit by a model wherein fibrils were composed of six laterally associated filaments. The chosen model parameters are summarized in Table 2.

TABLE 2 Model parameters

Parameter	Value
K_{MD}	0.64 ± 0.08 μM^{-1}
k_M/k_I	80 ± 30 μM
k_D/k_I	0.65 ± 0.15
k_n/k_p	$1.7 \pm 0.1 \times 10^{-6}$ μM^{-4}
k_{la}	$4.7 \pm 0.3 \times 10^{-3}$ μM^{-2} h^{-1}
$\delta\omega_{fil}$	$9.8 \pm 0.9 \times 10^{-10}$ cm-rad
$\delta\omega_{fib}$	$1.06 \pm 0.03 \times 10^{-8}$ cm-rad
n	6
p	6
q	3

Model simulations and evaluation

Fibril growth at 70, 140, and 280 μM Aβ was simulated using the model and the parameter set given in Table 2. The data and simulations are shown in Fig. 8. The model does very well in accurately simulating the increase in d_{sph} with time at all three concentrations (Fig. 8, *A* and *B*). The model captures the shape of $I_s(90°)$ data versus time quite well (Fig. 8, *C* and *D*), but misses slightly in absolute terms at 70 μM (all times) and at 280 μM (long times). $I_s(90°)$ values are very sensitive to total peptide concentration, and the relationship between d_{sph} and $I_s(90°)$ is very sensitive to the assumed filament diameter. A small error in either would lead to a relatively large error in the absolute value of $I_s(90°)$, which likely explains the differences between model and data at 70 μM. An additional complication arises due to the manner in which fibril length was calculated. To calculate the relationship between M_F and L_F, we assumed that the effective cross-sectional area was $\pi\, p\, d_f^2$, where d_f is filament length (Eq. 24). A different relationship would be obtained if we used $\pi\, d_F^2$, where d_F is the fibril diameter. Physically, this could be explained as twisting and coiling of the fibril after filament lateral association; however, we had no direct means to quantify this phenomenon. Such compaction of fibrils would change the relationship between d_{sph} and $I_s(90°)$ in the case where fibrils are a significant fraction of the aggregated material, and thus may explain

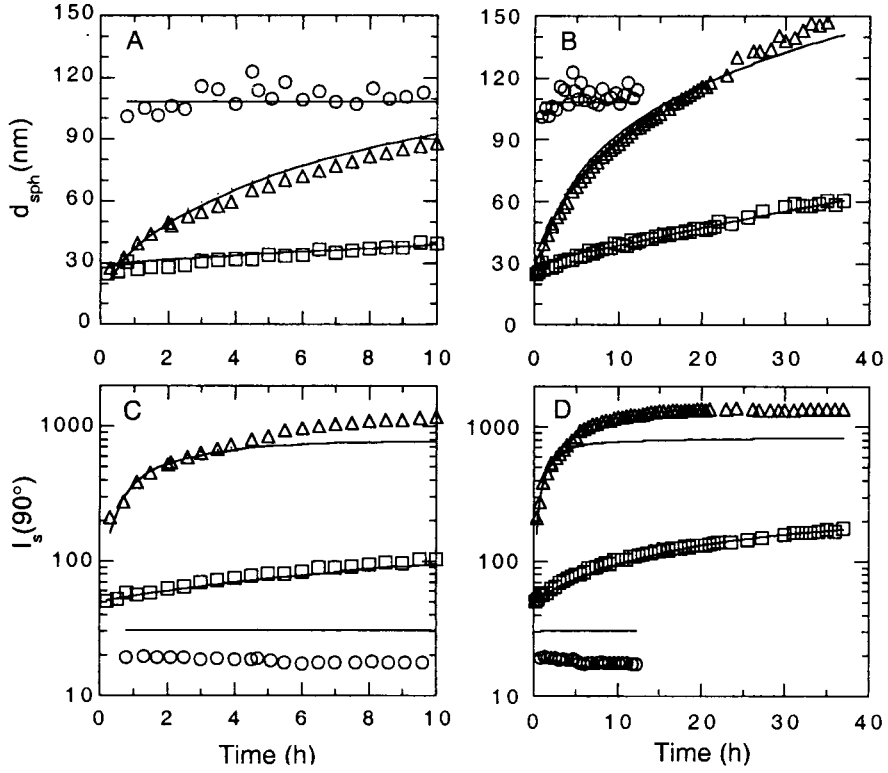

FIGURE 8 Measured average hydrodynamic diameter d_{sph} and average scattered intensity $I_s(90°)$ of Aβ aggregates at 70 μM (○), 140 μM (□), and 280 μM (△) are shown along with model simulations (*lines*) generated using parameters given in Table 2.

the discrepancy between simulation and data at longer times with 280 μM.

Next, we used the model to gain insight into growth patterns for filaments and fibrils, information that is difficult to access directly by experiment. The parameters given in Table 2 were used, and simulations were run at 70, 140, and 280 μM. In Fig. 9, we plot the weight fraction of Aβ in filament and fibril form, and the filament and fibril length, as a function of time and concentration. At 70 μM, virtually all the aggregated peptide exists as filaments. As concentration increases, the distribution shifts toward fibrils, and the time frame over which fibrils form decreases (Fig. 9, *A* and *B*). Qualitatively, these simulations are in agreement with bis-ANS data, if we assume that filaments bind less of the fluorescent dye than do fibrils. Filaments at 70 μM are much longer than those found at the higher concentrations (Fig. 9 *C*), and initial filament size decreases with increasing concentration. This pattern is due to the competition between nucleus formation and filament elongation, both of which consume *I*. Over longer time, filament size tends to the same value, ~200 nm, at both 140 and 280 μM. Fibrils are only slightly longer than filaments at 140 μM, whereas at 280 μM fibrils grow considerably longer, indicating that fibril elongation becomes a dominant growth mechanism only at higher concentrations.

We simulated the behavior at Aβ concentrations below 70 μM (Fig. 10). Interestingly, the concentration of *I* becomes measurable only at ~10 μM total Aβ and reaches a maximum at ~25 μM total Aβ. Below this point, less unfolded monomer is converted to *I* and the concentration of *I* is insufficient to drive significant further aggregation. Above this point, further association into *N*, filaments, and fibrils is favored. This gives an overall "critical concentration" for high-molecular-weight aggregates of ~20 μM. These predicted values are very close to experimental values reported by others (Soreghan et al., 1994; Huang et al., 2000).

We examined the necessity of including filament and fibril elongation and lateral association in our model. We refit the data with one kinetic parameter ($\delta\omega_{fil}$, $\delta\omega_{fib}$, or k_{la}) set equal to zero. The model was unable to converge without the fibril elongation step, justifying inclusion of fibril elongation as a necessary growth mechanism. Without lateral association, model simulations were unable to capture the experimental data at the two higher concentrations (not shown). Excluding filament elongation ($\delta\omega_{fib} = 0$) was less problematic; the observed plateau for $I_s(90°)$ at 280 μM is more closely approached, but at the expense of capturing the rate of increase in $I_s(90°)$ at early times (not shown). Thus, filament elongation makes a minor, almost negligible, contribution to the aggregation pathway. Interestingly, in AFM

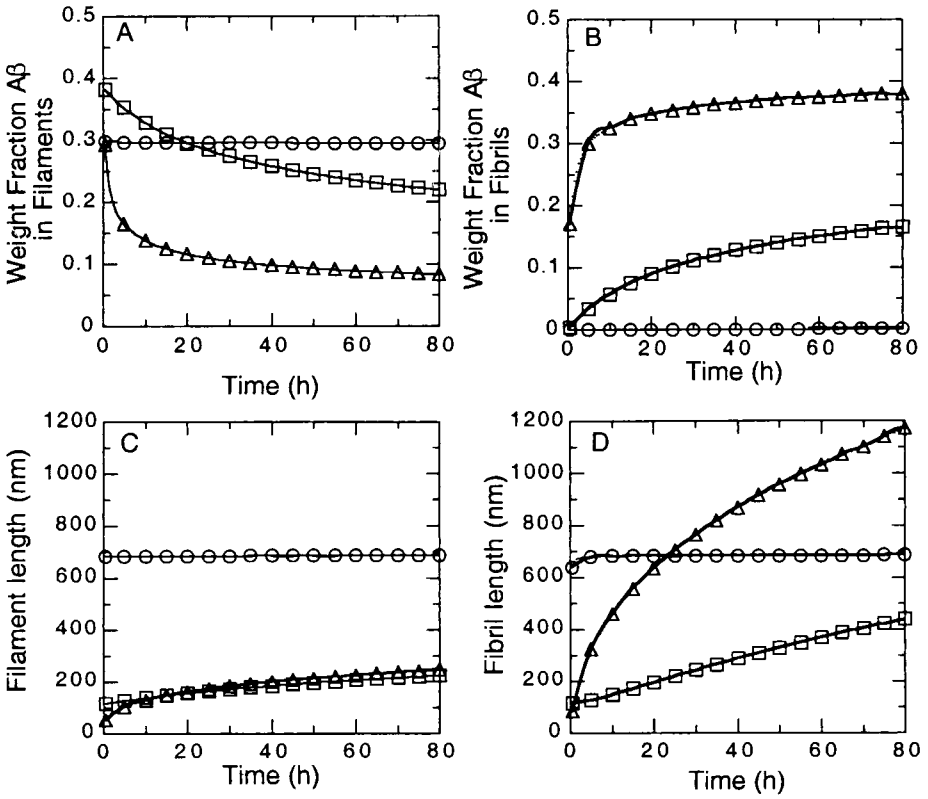

FIGURE 9 Model simulations using parameters given in Table 2. (*A*) Weight fraction of total Aβ present as filaments, (*B*) weight fraction of total Aβ present as fibrils, (*C*) average filament length, and (*D*) average fibril length for 70 μM (○), 140 μM (□), and 280 μM (△).

studies Harper et al. (1999) suggested that filament elongation was much slower than fibril elongation.

Relationship of Aβ aggregation state to Aβ toxicity

To examine whether our kinetic model could provide insight into mechanisms of Aβ toxicity, we prepared Aβ solutions by urea denaturation followed by dilution into PBSA at 70, 140, and 280 μM. Samples were aggregated for 1 or 3 days at room temperature, then applied to plated PC-12 cells at a constant final Aβ concentration of 35 μM. Cell toxicity was ascertained by MTT reduction assay after 24 h exposure. As shown in Fig. 11, toxicity decreased with increasing aggregation concentration and, to a lesser extent, increasing aggregation time. We used the model to simulate Aβ aggregation at the three different concentrations, and compared simulations to toxicity data. The strongest correlation was observed between cell toxicity and fraction of aggregated Aβ present as filaments (Fig. 11). At 70 μM, as shown in more detail in Fig. 9, ~30% of Aβ was aggregated, and virtually all the aggregated peptide was present as filaments; this sample was extremely toxic, with cell viability only ~3% of control (untreated) wells. At 280 μM, nearly 50% of the Aβ was aggregated, but much of this (75–80%) was fibrils. This sample was much less toxic to the cells. This correlation suggests that the filament form of Aβ is the toxic species.

DISCUSSION

Deposition of Aβ as insoluble fibrillar aggregates is one of the defining pathological features of Alzheimer's disease, and a number of epidemiological, genetic-linkage, and transgenic mouse studies indicate that Aβ deposition is causally linked to neurodegeneration. Early in vitro studies indicated the requirement of aggregation for Aβ toxicity (Pike et al., 1993; Simmons et al., 1994; Lorenzo and Yankner, 1994; Seilheimer et al., 1997). In more recent years an alternative hypothesis has gained exposure, namely that a soluble intermediate in the fibrillogenesis pathway, not the final insoluble product, is the toxic moiety (Pallitto et al., 1999; Lansbury, 1999; Koo et al., 1999). As examples, dimeric (Roher et al., 1996), oligomeric (Lambert et al., 1998), and "protofibrillar" Aβ (Hartley et al., 1999; Ward et al., 2000) are reportedly toxic to cultured cells. Additionally, Aβ fibrils pre-deposited onto a solid surface were not toxic to neurons, even though solutions of Aβ fibrils were toxic (Wujek et al., 1996).

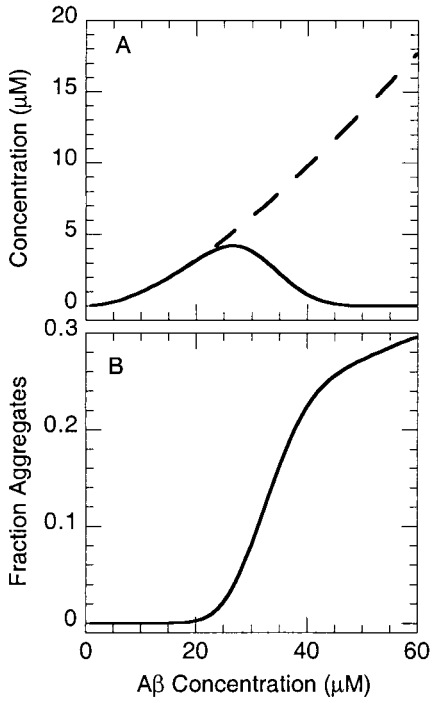

FIGURE 10 Model simulations at low concentrations, using parameters given in Table 2. (*A*) Concentration of *I* (*solid line*) and of amyloidogenic Aβ (*I* + *N* + filaments + fibrils, *dashed line*), in equivalent monomer concentration, as a function of total Aβ concentration. (*B*) Weight fraction of aggregates (filaments + fibrils) as a function of total Aβ concentration.

Given the biological relevance of Aβ fibrillogenesis, the pathway and kinetics by which Aβ monomers form fibrils have been the subject of investigation (see Murphy and Pallitto, 2000, for brief review). Jarrett et al. (1993) proposed a qualitative kinetic model for Aβ self-association which included a lag phase, a rapid growth phase, and then a plateau phase. Tomski and Murphy (1992) derived a quantitative model that described the kinetics of fibril elongation. Naiki and Nakakuki (1996) proposed that fibrils elongated by reversible addition of monomer to preexisting fibrils and derived a simple mathematical model. Lomakin et al. (1996, 1997) published the most detailed mathematical model to date. Briefly, monomers were postulated to rapidly and reversibly form micelles from which nuclei slowly but irreversibly emerged; fibrils elongated by addition of monomer to nuclei or other fibrils. This model accounts for the presence of both monomer and fibrillar forms, and can predict both the mass concentration of fibrils and fibril length as a function of time. However, the experiments upon which the model was based were conducted at nonphysiological conditions (pH ~ 1). None of the published kinetic models distinguishes between filaments and fibrils, or accounts for conversion between these two states. Yet, based on atomic force microscopy observation, Harper et al. (1999) suggested that lateral aggregation of filaments into fibrils is a key, perhaps rate-limiting, step in the assembly process.

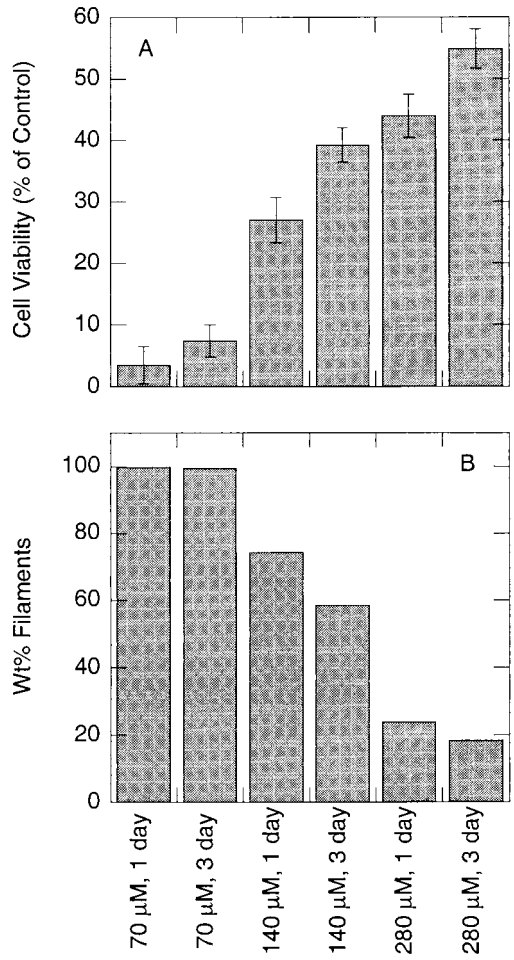

FIGURE 11 (*A*) Cell viability for Aβ-treated PC-12 cells, assessed using the MTT assay. Aβ was solubilized in 8 M urea, pH 10, diluted into PBSA, aggregated at the indicated concentration and time, then diluted to 35 μM and added to plated PC-12 cells. (*B*) Wt % aggregated Aβ in filament form, calculated from the kinetic model at the indicated concentration and time.

In this work we developed a comprehensive mathematical model of the kinetics of Aβ aggregation that is consistent with numerous experimental observations. This model is a significant improvement over previous mathematical models for several reasons: 1) experiments were performed at physiological pH, 2) initiation and growth mechanisms were included, 3) both monomer addition and fibril-fibril association were included as growth mechanisms, 4) both filaments and fibrils were included, and 5) mass fractions and filament/fibril lengths are modeled.

A key feature of our model is the hypothesis that unfolded Aβ, upon dilution into a "folding" buffer, rapidly and irreversibly partitions between two pathways. One pathway produces monomers and dimers of stable (but undefined) structure. Indeed, recent studies suggest that at low concentrations (<20 μM), Aβ forms a mix of monomers, dimers, and tetramers lacking regular secondary structural features (Huang et al., 2000). The other pathway generates an un-

stable intermediate that aggregates further. Aβ species in this branch are likely β-sheet-containing oligomers (Barrow et al., 1992). Our simulations predict a narrow concentration range over which a β-sheet dimeric intermediate would exist in the absence of significant highly aggregated species. Partitioning between a non-amyloidogenic ("on") pathway and an amyloidogenic ("off") pathway is a unique feature of our mathematical model, although experimental evidence for such a partitioning has been presented previously (Soto and Castano, 1996). Similarly, amyloid fibril formation from transthyretin is believed to proceed via formation of an alternatively folded conformation that is β-sheet rich (Lashuel et al., 1999). This result suggests that there is a normal "folded" Aβ structure; possibly, this stable structure has a normal physiological function. Using our model, we calculate that at 10 nM Aβ, >99% of the peptide is stable monomer, while at 10 μM Aβ, ~10% of the peptide is in the "amyloidogenic" pathway.

A second unique feature of our mathematical model is the explicit inclusion of both filaments and fibrils as distinct aggregated forms of Aβ. Several investigators have observed both filaments (linear aggregates of ~3–4 nm diameter) and fibrils (linear aggregates of ~8–12 nm diameter) using electron microscopy, atomic force microscopy, and x-ray diffraction (e.g., Fraser et al., 1991; Harper et al., 1997, 1999; Malinchik et al., 1998). Our model is consistent with these structural observations. Furthermore, the number of filaments per fibril extracted from our model fit ($p = 6$) is consistent with experimental observations (Fraser et al., 1991; Malinchik et al., 1998).

Conversion of unstable intermediate to larger aggregates is proposed to proceed via four steps: initiation via cooperative association of intermediate, elongation by addition of monomer to filament, lateral aggregation of filament to fibril, and elongation by end-to-end association of shorter fibrils or filaments. All four of these steps are consistent with our experimental evidence and that obtained by AFM (Harper et al., 1999). Both the initial size of aggregates and the rate of growth are highly concentration-dependent. This is evidence of the highly cooperative nature of Aβ fibril formation and growth. Our data were best fit by a sixth-order reaction for conversion of intermediate to nucleus (fibril initiation) and a third-order reaction for conversion of filaments to fibrils (lateral aggregation). The two mechanisms for elongation, monomer addition and end-to-end association of smaller fibrils, are both second-order reactions. Thus, at lower concentrations, elongation is relatively more important and a few long filaments are produced, whereas at higher concentrations, initiation and lateral aggregation become more dominant features.

The model specifically applies to the situation where Aβ starts in the urea-denatured state. We chose this to ensure that the initial state of Aβ was defined as fully monomeric and unfolded. The model could easily be adapted to simulate alternative initial conditions. The secondary structure and state of aggregation of Aβ is a strong function of the solvent in which it is dissolved (Barrow et al., 1992; Shen and Murphy, 1995; Thunecke et al., 1998). We suspect that the fraction of material committed to the "on" versus the "off" pathway is very sensitive to the manner in which it is treated, i.e., the peptide's history. This affects the initial distribution of monomeric, dimeric, intermediate, and other species. This, coupled with the strong concentration dependence, may explain the markedly different results obtained by using different solvents for dissolution, and the batch-to-batch and lab-to-lab variability reported by investigators of Aβ aggregation. Residual urea in the final solution could affect Aβ conformation or aggregation kinetics, perhaps by binding to the surface of aggregated peptide. We have previously published data on kinetics of Aβ growth from the DMSO-denatured state (Kremer et al., 2000). Preliminary analysis of the data in light of our mathematical model suggests that the split between the "on" and "off" pathways, and k_n/k_p, are not significantly affected by the change from DMSO to urea, but k_{la} is greater. We speculate that this indicates that residual urea inhibits lateral aggregation of filaments into fibrils; more detailed analysis and experimentation is underway.

As with any model, some simplifications were needed that may limit the range over which extrapolations are feasible. In particular, we assumed several reactions were irreversible, or nearly so. There are no mathematical difficulties that prevent incorporation of reversible reactions into the model; what is missing are experimental data that allow values for these parameters to be uniquely fit. Another limitation is that the model (and the experimental data from which it was derived) is restricted to a single phase. A further refinement of the model would include heterogeneous association between Aβ in solution and Aβ deposited as a solid phase. There is clear evidence that such association exists and is likely an important mechanism for growth of amyloid deposits in vivo (Tseng et al., 1999; Esler et al., 2000).

The nonlinear nature of the system (high reaction order, and participation of species in multiple steps) means that it is difficult, if not impossible, to characterize or predict Aβ aggregation kinetics without a mathematical model. Simulations can provide insights into experimentally inaccessible time frames or concentrations. For example, most biophysical studies of Aβ kinetics are conducted with concentrations in the μM range, on a time scale of minutes to days, whereas the concentration of soluble Aβ in cerebrospinal fluid is nanomolar, with aggregation and deposition taking place over years. Extrapolation of a model derived from data taken under experimentally accessible conditions to physiologically relevant conditions is hazardous, yet may be the only reasonable way to mimic the in vivo situation. The model can easily be modified to simulate other conditions of interest (e.g., addition of preformed fibrils to Aβ monomers.)

Quantitative kinetic models such as the one developed here can serve as useful tools to validate or refute hypotheses regarding the mechanism of toxicity of Aβ. In our experiments, toxicity was strongly dependent on the aggregation concentration, even though the final Aβ concentration to which cells were exposed was identical. Based on our model simulations, we speculate that long soluble filaments are the predominant toxic species. Other published results are consistent with our findings. Wujek et al. (1996) reported that fibril solutions, not fibrillar deposits, were toxic. Ward et al. (2000) fractionated aged Aβ and reported that toxicity was restricted to fractions containing "protofibrils" (rod-like structures 3–4 nm in diameter) and mature fibrils (longer branched fibrillar structures 6–12 nm in diameter). Interestingly, the protofibril-enriched fractions were toxic at much lower (equivalent monomer) concentrations than the mature fibrils. We have previously demonstrated that peptidyl inhibitors that increase Aβ aggregation kinetics and decrease time to formation of precipitates also protect cells from Aβ toxicity (Ghanta et al., 1996; Pallitto et al., 1999; Lowe et al., 2001). We speculate that such inhibitors accelerate the rate of conversion of filaments to fibrils and fibrillar deposits.

Many natural and synthetic compounds have been suspected of enhancing or inhibiting Aβ aggregation. This list includes: glycosaminoglycans (McLaurin et al., 1999), α_2-macroglobulin (Hughes et al., 1998), high density lipoprotein (Olesen and Dago, 2000), apolipoprotein E (Ma et al., 1994), Beffert and Poirier, 1998); gangliosides (Choo-Smith and Surewicz, 1997), metal ions (Bush et al., 1994), tetracyclic compounds (Howlett et al., 1999), pyridones (Kuner et al., 2000), peptides (Ghanta et al., 1996; Soto et al., 1996; Tjernberg et al., 1997; Findeis et al., 1999), and detergents (Wood et al., 1996). Compounds could variously prevent, slow, or accelerate the rates of nucleation, lateral association, or elongation, or could change partitioning between amyloidogenic and nonamyloidogenic pathways. The mode of action can be identified by combining our kinetic model with appropriate experimental data. Such analysis would be beneficial in identifying compounds that increase or inhibit the propensity of Aβ to form toxic aggregated species. Additionally, identification of the key steps involved in regulating the distribution of Aβ species should aid in developing novel compounds of therapeutic value.

This work was supported by National Institutes of Health grant AG14079 from the National Institute on Aging and by National Institutes of Health Molecular Biophysics Training Grant 5T32 GM08293-09 (to M.M.P.). We thank Andrea Strzelec for completing the toxicity experiments.

REFERENCES

Barrow, C. J., A. Yasuda, P. T. Kenny, and M. G. Zagorski. 1992. Solution conformations and aggregational properties of synthetic amyloid β peptides of AD. *J. Mol. Biol.* 225:1075–1093.

Beffert, U., and J. Poirier. 1998. ApoE associated with lipid has a reduced capacity to inhibit β-amyloid fibril formation. *NeuroReport.* 9:3321–3323.

Billmeyer, F. W. 1971. Textbook of Polymer Science, 2nd Ed. John Wiley & Sons, Inc., New York.

Burchard, W. 1983. Static and dynamic light scattering from branched polymers and biopolymers. *Adv. Polym. Sci.* 48:4–124.

Burdick, D., B. Soreghan, M. Kwon, J. Kosmoski, M. Knauer, A. Henscher, T. Yates, C. Cotman, and C. Glabe. 1992. Assembly and aggregation properties of synthetic Alzheimer's A4/β amyloid peptide analogs. *J. Biol. Chem.* 267:546–554.

Bush, A. I., W. H. Pettingell, G. Multhaup, M. Paradis, J. P. von Sattel, J. F. Gusella, K. Beyreuther, C. L. Masters, and R. E. Tanzi. 1994. Rapid induction of Alzheimer A beta amyloid formation by zinc. *Science.* 265:1464–1467.

Caracotsios, J., and W. E. Stewart. 1985. Sensitivity analysis of initial value problems with mixed ODEs and algebraic equations. *Comp. Chem. Eng.* 9:359–365.

Chiti, F., N. Taddei, M. Bucciantini, P. White, G. Ramponi, and C. M. Dobson. 2000. Mutational analysis of the propensity for amyloid formation by a globular protein. *EMBO J.* 19:1441–1449.

Choo-Smith, L. P., and W. K. Surewicz. 1997. The interaction between Alzheimer amyloid β(1-40) peptide and ganglioside GM1-containing membranes. *FEBS Lett.* 402:95–98.

Creighton, T. E. 1994. The protein folding problem. *In* Mechanisms of Protein Folding. R. H. Pain, editor. Oxford University Press, New York.

Davies, O. C. 1954. Design and Analysis of Industrial Experiments. Hafner Publishing Co., New York.

Esler, W. P., E. R. Stimson, J. M. Jennings, H. V. Vinters, J. R. Ghilardi, J. P. Lee, P. W. Mantyh, and J. E. Maggio. 2000. Alzheimer's disease amyloid propagation by a template-dependent dock-lock mechanism. *Biochemistry.* 39:6288–6295.

Findeis, M. A., G. M. Musso, C. C. Arico-Muendel, H. W. Benjamin, A. M. Hundal, J.-J. Lee, J. Chin, M. Kelley, J. Wakefield, N. J. Hayward, and S. M. Molineaux. 1999. Modified-peptide inhibitors of amyloid β-peptide polymerization. *Biochemistry.* 38:6791–6800.

Fink, A. L. 1998. Protein aggregation: folding aggregates, inclusion bodies, and amyloid. *Fold. Des.* 3:R1–R9.

Fraser, P. E., L. K. Duffy, M. B. O'Malley, J. Nguyen, H. Inouye, and D. A. Kirschner. 1991. Morphology and antibody recognition of synthetic beta-amyloid peptides. *J. Neurosci. Res.* 28:474–485.

Games, D., D. Adams, R. Alessandrini, R. Barbour, P. Berthelette, C. Blackwell, T. Carr, J. Clemens, T. Donaldson, F. Gillepsie, T. Guido, S. Hagopian, K. Johnson-Wood, K. Khan, M. Lee, P. Leibowitz, I. Lieberburg, S. Little, E. Masliah, L. McConlogue, M. Montoya-Zavala, L. Mucke, L. Paganini, E. Penniman, M. Power, D. Schenk, P. Seubert, B. Snyder, F. Soriano, H. Tan, J. Vitale, S. Wadsworth, B. Wolozin, and J. Zhao. 1995. Alzheimer-type neuropathology in transgenic mice overexpressing V717F β-amyloid precursor protein. *Nature.* 373:523–527.

Ghanta, J., C.-L. Shen, L. L. Kiessling, and R. M. Murphy. 1996. A strategy for designing inhibitors of β-amyloid toxicity. *J. Biol. Chem.* 271:29525–29528.

Gibbons, D. L., and P. M. Horowitz. 1995. Exposure of hydrophobic surfaces on the chaperonin GroEL oligomer by protonation or modification of His-401. *J. Biol. Chem.* 270:7335–7340.

Glenner, G. G., and C. W. Wong. 1984. Alzheimer's disease and Down's syndrome: sharing of a unique cerebrovascular amyloid fibril protein. *Biochem. Biophys. Res. Commun.* 122:1131–1135.

Goldberg, M. E., R. Rudolph, and R. Jaenicke. 1991. A kinetic study of the competition between renaturation and aggregation during refolding of denatured-reduced egg white lysozyme. *Biochemistry.* 30:2790–2797.

Harper, J. D., S. S. Wong, C. M. Lieber, and P. T. Lansbury, Jr. 1997. Observation of metastable Aβ amyloid protofibrils by atomic force microscopy. *Chem. Biol.* 4:119–125.

Harper, J. D., S. S. Wong, C. M. Lieber, and P. T. Lansbury, Jr. 1999. Assembly of Aβ amyloid protofibrils: an in vitro model for a possible early event in Alzheimer's disease. *Biochemistry.* 38:8972–8980.

Hartley, D. M., D. M. Walsh, C. P. Ye, T. Diehl, S. Vasquez, P. M. Vassilev, D. B. Teplow, and D. S. Selkoe. 1999. Protofibrillar intermediates of amyloid β-protein induce acute electrophysiological changes and progressive neurotoxicity in cortical neurons. *J. Neurosci.* 19: 8876–8884.

Hill, T. L. 1983. Length dependence of rate constants for end-to-end association and dissociation of equilibrium linear aggregates. *Biophys. J.* 44:285–288.

Holcomb, L., M. N. Gordon, E. McGowan, X. Yu, S. Benkovic, P. Jantzen, K. Wright, I. Saad, R. Mueller, D. Morgan, S. Sanders, C. Zehr, K. O'Campo, J. Hardy, C.-M. Prada, C. Eckman, S. Younkin, K. Hsiao, and K. Duff. 1998. Accelerated Alzheimer-type phenotype in transgenic mice carrying both mutant amyloid precursor protein and presenilin-1 transgenes. *Nature Med.* 4:97–100.

Howlett, D. R., A. R. George, D. E. Owen, R. V. Ward, and R. E. Markwell. 1999. Common structural features determine the effectiveness of carvedilol, daunomycin and rolitetracycline as inhibitors of Alzheimer β-amyloid fibril formation. *Biochem. J.* 343:419–423.

Hsiao, K., P. Chapman, S. Nilsen, C. Eckman, Y. Harigaya, S. Younkin, F. Yang, and G. Cole. 1996. Correlative memory deficits, Aβ elevation, and amyloid plaques in transgenic mice. *Science.* 274:99–102.

Huang, T. H. J., D.-S. Yang, N. P. Plaskos, S. Go, C. M. Yip, P. E. Fraser, and A. Chakrabartty. 2000. Structural studies of soluble oligomers of the Alzheimer β-amyloid peptide. *J. Mol. Biol.* 297:73–87.

Hughes, S. R., O. Khorkava, S. Goyal, J. Knaeblein, J. Heroux, N. G. Riedel, and S. Sahasrabudhe. 1998. α_2-Macroglobulin associates with β-amyloid peptide and prevents fibril formation. *Proc. Natl. Acad. Sci. USA.* 95:3275–3280.

Jarrett, J. T., E. P. Berger, and P. T. Lansbury, Jr. 1993. The carboxy terminus of the β amyloid protein is critical for the seeding of amyloid formation: implications for the pathogenesis of Alzheimer's disease. *Biochemistry.* 32:4693–4697.

Joachim, C. L., and D. J. Selkoe. 1992. The seminal role of β-amyloid in the pathogenesis of Alzheimer disease. *Alzheimer Dis. Assoc. Disord.* 6:7–34.

Kang, J., H.-G. Lemaire, A. Unterbeck, J. M. Salbaum, C. L. Masters, K.-H. Grzeschik, G. Multhaup, K. Beyreuther, and B. Muller-Hill. 1987. The precursor of Alzheimer's disease amyloid A4 protein resembles a cell-surface receptor. *Nature.* 325:733–736.

Koo, E. H., P. T. Lansbury, Jr., and J. W. Kelley. 1999. Amyloid diseases: abnormal protein aggregation in neurodegeneration. *Proc. Natl. Acad. Sci. USA.* 96:9989–9990.

Kowaleski, T., and D. M. Holtzman. 1999. In situ atomic force microscopy study of Alzheimer's beta-amyloid peptide on different substrates: new insights into mechanism of beta-sheet formation. *Proc. Natl. Acad. Sci. USA.* 96:3688–3693.

Koyama, R. 1973. Light scattering of stiff chain polymers. *J. Phys. Soc. Jpn.* 34:1029–1038.

Kremer, J. J., M. M. Pallitto, D. J. Sklansky, and R. M. Murphy. 2000. Correlation of β-amyloid aggregate size and hydrophobicity with decreased bilayer fluidity of model membranes. *Biochemistry.* 39: 10309–10318.

Kuner, P., B. Bohrmann, L. O. Tjernberg, J. Naslund, G. Huber, S. Celenk, F. Gruninger-Leitch, J. G. Richards, R. Jakob-Roetne, J. A. Kemp, and C. Nordstedt. 2000. Controlling polymerization of β-amyloid and prion-derived peptides with synthetic small molecule ligands. *J. Biol. Chem.* 275:1673–1678.

Lambert, M. P., A. K. Barlow, B. A. Chromy, C. Edwards, R. Freed, M. Liosatos, T. E. Morgan, I. Rozovsky, B. Trommer, K. L. Viola, P. Wals, C. Zhang, C. E. Finch, G. A. Krafft, and W. L. Klein. 1998. Diffusible, nonfibrillar ligands derived from Abeta (1-42) are potent central nervous system neurotoxins. *Proc. Natl. Acad. Sci. USA.* 95:6448–6453.

Lansbury, P. T., Jr. 1999. Evolution of amyloid: what normal protein folding may tell us about fibrillogenesis and disease. *Proc. Natl. Acad. Sci. USA.* 96:3342–3344.

Lashuel, H. A., C. Wurth, L. Woo, and J. W. Kelly. 1999. The most pathogenic transthyretin variant, L55P, forms amyloid fibrils under acidic conditions and protofilaments under physiological conditions. *Biochemistry.* 38:13560–13573.

Lomakin, A., D. S. Chung, G. B. Benedek, D. A. Kirschner, and D. B. Teplow. 1996. On the nucleation and growth of amyloid β-protein fibrils: detection of nuclei and quantitation of rate constants. *Proc. Natl. Acad. Sci. USA.* 93:1125–1129.

Lomakin, A., D. B. Teplow, D. A. Kirschner, and G. B. Benedek. 1997. Kinetic theory of fibrillogenesis of amyloid β-protein. *Proc. Natl. Acad. Sci. USA.* 94:7942–7947.

Lorenzo, A., and B. A. Yankner. 1994. Beta-amyloid neurotoxicity requires fibril formation and is inhibited by Congo red. *Proc. Natl. Acad. Sci. USA.* 91:12243–12247.

Lowe, T. L., A. Strzelec, L. L. Kiessling, and R. M. Murphy. 2001. Structure–function relationships for inhibitors of β-amyloid toxicity containing the recognition sequence KLVFF. *Biochemistry.* 40: 7882–7889.

Ma, J., A. Yee, H. B. Brewer, Jr., S. Das, and H. Potter. 1994. Amyloid-associated proteins α_1-antichymotrypsin and apolipoprotein E promote assembly of Alzheimer β-protein into filaments. *Nature.* 372:92–94.

Malinchik, S. B., H, Inouye, K. E. Szumowski, and D. A. Kirschner. 1998. Structural analysis of Alzheimer's β(1-40) amyloid: protofilament assembly of tubular fibrils. *Biophys. J.* 74:537–545.

Masters, C. L., G. Simms, N. A. Weinman, G. Multhaup, B. L. McDonald, and K. Beyreuther. 1985. Amyloid plaque core proteins in Alzheimer disease and Down syndrome. *Proc. Natl. Acad. Sci. USA.* 82:4245–4249.

Mattson, M. P., B. Cheng, D. David, K. Bryant, I. Lieberburg, and R. E. Rydel. 1992. β-Amyloid peptides destabilize calcium homeostasis and render human cortical neurons vulnerable to excitotoxicity. *J. Neurosci.* 12:376–389.

McLaurin, J., T. Franklin, X. Zhang, J. Deng, and P. E. Fraser. 1999. Interactions of Alzheimer amyloid-β peptides with glycosaminoglycans. *Eur. J. Biochem.* 266:1101–1110.

Murphy, R. M., and M. M. Pallitto. 2000. Probing the kinetics of beta-amyloid self-association. *J. Struct. Biol.* 130:109–122.

Naiki, H., and K. Nakakuki. 1996. First-order kinetic model of Alzheimer's β-amyloid fibril extension in vitro. *Lab. Invest.* 74:374–383.

Olesen, O. F., and L. Dago. 2000. High density lipoprotein inhibits assembly of amyloid β-peptides into fibrils. *Biochem. Biophys. Res. Commun.* 270:62–66.

Pallitto, M. M., J. Ghanta, P. Heinzelman, L. L. Kiessling, and R. M. Murphy. 1999. Recognition sequence design for peptidyl modulators of β-amyloid aggregation and toxicity. *Biochemistry.* 38:3570–3578.

Pike, C. J., D. Burdick, A. J. Walencewicz, C. G. Glabe, and C. W. Cotman. 1993. Neurodegeneration induced by β-amyloid peptides in vitro: the role of peptide assembly state. *J. Neurosci.* 13:1676–1687.

Roher, A. E., M. O. Chaney, Y.-M. Kuo, S. D. Webster, W. B. Stine, L. J. Haverkamp, A. S. Woods, R. J. Cotter, J. M. Tuohy, G. A. Krafft, B. S. Bonnell, and M. R. Emmerling. 1996. Morphology and toxicity of Aβ-(1-42) dimer derived from neuritic and vascular amyloid deposits of Alzheimer's disease. *J. Biol. Chem.* 271:20631–20635.

Schmidt, L. 1998. The Engineering of Chemical Reactions. Oxford University Press, New York.

Seilheimer, B., B. Bohrmann, L. Bondolfi, F. Muller, D. Stuber, and H. Dobeli. 1997. The toxicity of the Alzheimer's β-amyloid peptide correlates with a distinct fiber morphology. *J. Struct. Biol.* 119:59–71.

Shen, C.-L., M. C. Fitzgerald, and R. M. Murphy. 1994. Effect of acid predissolution on fibril size and fibril flexibility of synthetic β-amyloid peptide. *Biophys. J.* 67:1238–1246.

Shen, C.-L., and R. M. Murphy. 1995. Solvent effects on self-assembly of β-amyloid peptide. *Biophys. J.* 69:640–651.

Simmons, L. K., P. C. May, K. J. Tomaselli, R. E. Rydel, K. S. Fuson, E. F. Brigham, S. Wright, I. Lieberburg, G. W. Becker, D. N. Brems, and W. Y. Li. 1994. Secondary structure of amyloid β peptide correlates with neurotoxic activity in vitro. *Mol. Pharmacol.* 45:373–379.

Soreghan, B., J. Kosmoski, and C. Glabe. 1994. Surfactant properties of Alzheimer's Aβ peptides and the mechanism of amyloid aggregation. *J. Biol. Chem.* 269:28551–28554.

Soto, C., and E. M. Castano. 1996. The conformation of Alzheimer's β-peptide determines the rate of amyloid formation and its resistance to proteolysis. *Biochem. J.* 314:701–707.

Soto, C., M. S. Kindy, M. Baumann, and B. Frangione. 1996. Inhibition of Alzheimer's amyloidosis by peptides that prevent β-sheet conformation. *Biochem. Biophys. Res. Commun.* 226:672–680.

Stewart, W. E. 1987. Multiresponse parameter estimation with a new and noninformative prior. *Biometrika.* 74:557–562.

Stine, W. B., S. W. Snyder, U. S. Ladror, W. S. Wade, M. F. Miller, T. J. Perun, T. F. Holzman, and G. A. Krafft. 1996. The nanometer-scale structure of amyloid-β visualized by atomic force microscopy. *J. Protein Chem.* 15:193–203.

Thunecke, M., A. Lobbia, U. Kosciessa, T. Dyrks, A. E. Oakley, J. Turner, W. Saenger, and Y. Georgalis. 1998. Aggregation of Aβ Alzheimer's disease-related peptide studied by dynamic light scattering. *J. Peptide Res.* 52:509–517.

Tjernberg, L. O., C. Lilliehook, D. J. E. Callaway, J. Naslund, S. Hahne, J. Thyberg, L. Terenius, and C. Norstedt. 1997. Controlling amyloid β-peptide fibril formation with protease-stable ligands. *J. Biol. Chem.* 272:12601–12605.

Tomski, S. J., and R. M. Murphy. 1992. Kinetics of aggregation of synthetic β-amyloid peptide. *Arch. Biochem. Biophys.* 294:630–638.

Tseng, B. P., W. P. Esler, C. B. Clish, E. R. Stimson, J. R. Ghilardi, H. V. Vinters, P. W. Mantyh, J. P. Lee, and J. E. Maggio. 1999. Deposition of monomeric, not oligomeric, Aβ mediates growth of Alzheimer's disease amyloid plaques in human brain preparations. *Biochemistry.* 38: 10424–10431.

Ward, R. V., K. H. Jennings, R. Jepras, W. Neville, D. E. Owen, J. Hawkins, G. Christie, J. B. Davis, A. George, E. H. Karran, and D. R. Howlett. 2000. Fractionation and characterization of oligomeric, protofibrillar and fibrillar forms of β-amyloid peptide. *Biochem. J.* 348: 137–144.

West, M. W., W. Wang, J. Patterson, J. D. Mancias, J. R. Beasley, and M. H. Hecht. 1999. De novo amyloid proteins from designed combinatorial libraries. *Proc. Natl. Acad. Sci. USA.* 96:11211–11216.

Wood, S. J., L. MacKenzie, B. Maleeff, M. R. Hurle, and R. Wetzel. 1996. Selective inhibition of Abeta fibril formation. *J. Biol. Chem.* 271: 4086–4092.

Wujek, J. R., M. D. Dority, R. C. A. Frederickson, and K. R. Brunden. 1996. Deposits of Aβ fibrils are not toxic to cortical and hippocampal neurons in vitro. *Neurobiol. Aging.* 17:107–113.

Yamakawa, H., and M. Fujii. 1973. Translational friction coefficient of wormlike chains. *Macromolecules.* 6:407–415.

Yankner, B. A., L. K. Duffy, and D. A. Kirschner. 1990. Neurotrophic and neurotoxic effects of amyloid β-protein: reversal by tachykinin neuropeptides. *Science.* 250:279–282.